EIGENSYSTEM REALIZATION OF VIOLIN BRIDGE ADMITTANCES

Riccardo Giampiccolo , Alessandro Ilic Mezza* , Raffaele Malvermi, Mirco Pezzoli, Alberto Bernardini, and Fabio Antonacci*

Image and Sound Processing Lab
Dipartimento di Elettronica, Informazione e Bioingegneria (DEIB), Politecnico di Milano, Milan, Italy
riccardo.giampiccolo@polimi.it

ABSTRACT

Modeling violin bridge admittance is a long-standing problem in musical acoustics, with applications in sound analysis, synthesis, and virtual instrument design. In this work, we investigate the use of the Eigensystem Realization Algorithm (ERA) for deriving reduced-order state-space models directly from measured impulse responses. The proposed approach allows us to extract dominant system dynamics and obtain compact realizations without requiring explicit modal parameterization. We evaluate ERA on a dataset of modern and historical violins and compare it against established modal and state-space identification methods. Experimental results demonstrate that ERA outperforms existing approaches by achieving lower reconstruction errors in both the time and frequency domains while preserving perceptually relevant characteristics of the bridge response. Furthermore, we show that the state-space realizations obtained using ERA reproduce the target frequency-dependent energy decay more accurately than models obtained using the baseline methods. These findings support the use of ERA as an efficient and flexible alternative for modeling violin bridge admittances, with applications that span from audio synthesis and processing to instrument virtualization.

1. INTRODUCTION

In the context of digital audio effects and sound synthesis, the accurate modeling of musical instruments remains a central challenge, especially when aiming for both accurate (i.e., physically-grounded) and controllable solutions [1]. Applications such as virtual instrument and real-time physical modeling require compact and efficient models capable of reproducing the interaction between excitation mechanisms and resonant structures. The case of the so-called *silent violin* is an emblematic example of the sort, where the final sound is indeed the result of the interplay between physical excitation and the digital model of the instrument body [2, 3, 4, 5], making the accurate characterization of its vibrational response essential for perceptual realism.

In this scenario, instruments of the violin family are typically characterized by means of their bridge admittance [6, 7, 8], which is used to derive efficient reduced-order models suitable for real-time sound synthesis [2, 3, 9, 10, 11] of the instrument. Indeed, the bridge plays a key role in the instrument dynamics as it acts as a mechanical interface transferring energy from the strings to the structure of the body [8]. In this context, the bridge admittance is providing a compact description of the local input-output relationship of the structure, linking the applied force to the resulting velocity response, and it is interpreted as the *signature* of a violin due to its connection with the design [12, 13], timbre [14, 7, 15] and directional sound [14, 16, 17] of the instrument.

Through the years, several methodologies have been proposed to derive parametric models of bridge admittances from measurements [11]. Classical approaches include IIR fitting techniques, which enable efficient digital implementations but may suffer from stability issues due to the lack of guaranteed passivity [18, 19]. To address these limitations, the vibrational behavior of violins has been extensively studied through modal analysis [20]. Prominent spectral peaks can indeed be attributed to individual modes, which can then be modeled as dampened harmonic oscillators. The extraction of modal parameters is typically carried out through multi-stage procedures [11]. These generally involve the identification of modal frequencies, amplitudes, and damping factors through, e.g., the filter diagonalization method [21], least-squares, nonlinear optimization, and, in some cases, solving convex programs to enforce physical constraints [2, 19, 22].

In this work, we propose an approach based on state-space system identification from measured bridge admittance impulse responses. In particular, we consider the Eigensystem Realization Algorithm (ERA), a well-known method originally developed at NASA in the context of structural dynamics [23, 24]. ERA provides a state-space realization through the singular value decomposition (SVD) of a Hankel matrix constructed directly from impulse response data. The method has been widely used for modal identification of mechanical systems and vibration analysis, where it enables the extraction of system poles and modal shapes from measured data in a compact and systematic manner [24]. To the best of our knowledge, ERA has not been previously applied to the problem of violin bridge admittance modeling. In contrast to existing approaches, the proposed method provides an algebraic matrix formulation of the identified state-space model, thereby avoiding the need for modal fitting procedures consisting of multiple sequential steps and offering a unified framework for parameter estimation with minimal heuristics.

ERA is evaluated against two methods from the literature [2], [3] on a dataset of bridge admittances of six violins, including five modern instruments selected from the collection of the “Antonio Stradivari International Triennial Competition,”[1] as well as a historical instrument crafted by Stradivari in the 18th century. Results show that ERA consistently outperforms the baseline methods across all considered measurements, achieving improved accuracy both in the time and frequency domains, as well as in the reconstruction of the frequency-dependent energy decay profiles.

The remainder of the paper is organized as follows. Section 2 reviews the methodologies relevant to violin bridge admittance

* R. Giampiccolo and A. I. Mezza contributed equally to this work.

[1] https://museodelviolino.org/en/concorso-triennale-2024/

modeling chosen as baselines, whereas Section 3 introduces the Eigensystem Realization Algorithm. Data acquisition and experimental results are presented in Section 4. Finally, conclusions are drawn in Section 5.

2. RELATED METHODS

Assuming that the bridge admittance $Y(z)$ can be described by a finite-dimensional proper rational representation, then there exists a discrete-time state-space model

$$\begin{aligned} \mathbf{x}[k+1] &= \mathbf{A}\mathbf{x}[k] + \mathbf{b}u[k]\,, \\ y[k] &= \mathbf{c}^{\mathrm{T}}\mathbf{x}[k] + du[k]\,, \end{aligned} \tag{1}$$

such that

$$Y(z) = \mathbf{c}^{\mathrm{T}}(z\mathbf{I} - \mathbf{A})^{-1}\mathbf{b} + d\,, \tag{2}$$

where $\mathbf{A} \in \mathbb{R}^{M\times M}$ is the state matrix, $\mathbf{b} \in \mathbb{R}^{M}$ is the input vector, $\mathbf{c} \in \mathbb{R}^{M}$ is the output vector, and $d \in \mathbb{R}$ is the direct feedthrough term. Hence, the problem of bridge admittance modeling can be recast into that of finding a realization $(\mathbf{A}, \mathbf{b}, \mathbf{c}, d)$.

In the context of state-space modeling of violins, Maestre *et al.* [3] recently proposed a method for the design of state-space filters for simulating the frequency-dependent sound source directivity from acoustic measurements, exciting the bridge with an impact hammer and measuring the sound pressure to obtain radiation responses. The method provides a compact and physically interpretable representation of the response data as a sum of exponentially decaying modes, where the poles encode modal frequencies and decay rates, and the modal gains determine their contribution. Although the original formulation targets direction-dependent radiation, when restricted to the case of a single impulse response, the same modal fitting strategy can be applied to find a suitable realization of the bridge admittance model in (2).

In [3], the state matrix is chosen in modal (diagonal) form

$$\mathbf{A} = \operatorname{diag}\left([p_1, \ldots, p_M]\right), \tag{3}$$

where $p_m \in \mathbb{C}$ are the system poles. In this case, since we consider a minimal realization, M is both the total number of poles and the total number of eigenvalues of $\mathbf{A}$. The authors fix $\mathbf{b} = \mathbf{1}$ and $d = 0$, since the feedthrough gain can be retrieved directly from the first sample of the measured impulse response $y[k]$, which is assumed to be minimum-phase. The transfer function (2) can be rewritten as

$$Y(z) = \sum_{m=1}^{M} c_m \frac{z^{-1}}{1 - p_m z^{-1}}\,, \tag{4}$$

and interpreted as a parallel bank of first-order resonant filters.

The poles p_m are estimated using an autoregressive (AR) all-pole model fitted on a frequency-warped version of the impulse response, $y_{\mathrm{w}}[k]$, obtained by mapping the unit circle in the z-plane onto the unit circle in the ζ-plane according to the conformal-map $z \leftarrow (\zeta + \rho)/(1 + \rho\zeta)$, with $\rho \in (0, 1)$ controlling the frequency warping. This allows us to derive the eigenvalues on a perceptually motivated frequency scale that provides a reliable estimation for relevant resonant modes of the modeled source. The warped-domain M eigenvalues are estimated as the roots of the polynomial $\mathbf{p} = [1, \alpha_1, \ldots, \alpha_M]$, which are then mapped back to the z-plane. In particular, given the AR model of the warped impulse response,

$$y_{\mathrm{w}}[\ell] \approx \sum_{m=1}^{M} \alpha_m y_{\mathrm{w}}[\ell - m]\,, \quad \ell = M, \ldots, L\,, \tag{5}$$

the coefficients α_m are obtained by solving a (weighted) least-squares problem [19].

Once the poles p_m are found, the impulse response can be expressed as a linear combination of modal basis functions

$$y[k] \approx \sum_{m=1}^{M} c_m h_m[k]\,, \tag{6}$$

where $h_m[k]$ is the impulse response of the m-th modal filter

$$H_m(z) = \frac{z^{-1}}{1 - p_m z^{-1}}\,. \tag{7}$$

The output vector $\mathbf{c} = [c_1, \ldots, c_M]^{\mathrm{T}}$ is obtained solving the least-squares problem

$$\min_{\mathbf{c}} \|\mathbf{y} - \mathbf{H}\mathbf{c}\|_2^2\,, \tag{8}$$

where $\mathbf{y} \in \mathbb{R}^{L}$ is the vector containing L samples of the impulse response, and $\mathbf{H} \in \mathbb{C}^{L\times M}$ contains the basis responses $h_m[k]$. Finally, collecting all the obtained parameters and imposing $d = y[0]$ yields a state-space realization in the form of (1).

To compare the previous approach with a more classical example of modal fitting, we now consider an earlier work from the same authors. In [2], Maestre *et al.* proposed a methodology to model bridge admittances from both one- and two-dimensional measurements. As for the one-dimensional case, they proposed to employ a parametric modal decomposition in the discrete-time domain, in which the measured admittance is approximated as a sum of second-order resonators. Denoting by $\hat{Y}(z)$ the estimated magnitude spectrum, the model reads as follows

$$\hat{Y}(z) = \sum_{m=1}^{M} g_m\, \tilde{H}_m(z)\,, \tag{9}$$

with modal gains $g_m \geq 0$ and modal response

$$\tilde{H}_m(z) = \frac{1 - z^{-2}}{(1 - p_m z^{-1})(1 - p_m^* z^{-1})}\,. \tag{10}$$

Then, every single mode is parameterized by the pair of complex conjugate poles, p_m and p_m^*, with

$$p_m = \exp(-\pi B_m/f_{\mathrm{s}}) \exp(j2\pi f_m/f_{\mathrm{s}})\,, \tag{11}$$

where f_m and B_m denote the modal frequency and bandwidth, respectively, and f_{s} is the sampling frequency.

To perform the fitting, the modal parameters are initialized by selecting peaks on the magnitude spectrum of the bridge admittance employing a peak-finding algorithm, with bandwidths estimated via the half-power method. In particular, the authors selected $M-1$ peaks between f_{min} and f_{max}, and just one single peak above f_{max} to model the highly damped peak (known as *bridge hill*) caused by the high overlap of modes at high frequency. The parameters are then refined by solving a nonlinear optimization problem over the vector

$$\xi = [f_1, \ldots, f_M,\, B_1, \ldots, B_M]^{\mathrm{T}}, \tag{12}$$

minimizing the cost function

$$\varepsilon(Y, \hat{Y}) = \sum_{k=1}^{K} \left| \log|Y[\omega_k]| - \log|\hat{Y}[\omega_k]| \right|\,, \tag{13}$$

which is subject to linear constraints enforcing $B_m > 0\ \forall\, m$, frequency ordering, and bounded search regions, with K being the total number of frequency bins and ω_k the discrete angular frequency at the k-th frequency bin. Once the modal parameters are fixed, the modal gains $\mathbf{g} = [g_1, \ldots, g_M]^{\mathrm{T}}$ are estimated by solving the constrained least-squares problem

$$\min_{\mathbf{g} \geq 0} \|\tilde{\mathbf{H}}\mathbf{g} - \tilde{\mathbf{y}}\|_2^2\,, \tag{14}$$

where $\tilde{\mathbf{H}} \in \mathbb{C}^{K \times M}$ is the modal basis matrix, whose rows contain K samples of $\tilde{H}_m(\omega)$, and $\tilde{\mathbf{y}} \in \mathbb{C}^K$ is a vector collecting K samples of $Y(\omega)$, with $0 < \omega < \pi$.

3. EIGENSYSTEM REALIZATION ALGORITHM

The Eigensystem Realization Algorithm (ERA) is a time-domain system identification method for constructing a reduced-order state-space model directly from impulse response data. Originally introduced by Juang and Pappa [23, 24] in the aerospace and structural dynamics fields for modal parameter identification from free-decay measurements, ERA can be viewed as an SVD-based extension of the Ho-Kalman realization algorithm [25]: it uses Markov parameters, i.e., the sequence of impulse response coefficients that characterize the system's input-output behavior, to recover a minimal realization of (1), whereas SVD truncation provides a practical mechanism for model order reduction by separating dominant dynamics from noise. In the following, we present the single-input single-output (SISO) formulation of ERA.

For a unit pulse input $u[k] = \delta[k]$ and zero initial condition $\mathbf{x}[0] = 0$, the system response $y[k]$ defines the Markov parameters

$$y[0] = d\,, \tag{15}$$

$$y[1] = \mathbf{c}^{\mathrm{T}}\mathbf{b}\,, \tag{16}$$

$$y[k] = \mathbf{c}^{\mathrm{T}}\mathbf{A}^{k-1}\mathbf{b}\,, \quad k \geq 2\,. \tag{17}$$

ERA constructs a Hankel matrix from these parameters:

$$\mathbf{H}_0 = \begin{bmatrix} y[1] & y[2] & \cdots & y[s] \\ y[2] & y[3] & \cdots & y[s+1] \\ \vdots & \vdots & \ddots & \vdots \\ y[r] & y[r+1] & \cdots & y[r+s-1] \end{bmatrix}, \tag{18}$$

along with the shifted Hankel matrix

$$\mathbf{H}_1 = \begin{bmatrix} y[2] & y[3] & \cdots & y[s+1] \\ y[3] & y[4] & \cdots & y[s+2] \\ \vdots & \vdots & \ddots & \vdots \\ y[r+1] & y[r+2] & \cdots & y[r+s] \end{bmatrix}, \tag{19}$$

with $r, s \in \mathbb{N}$ determining the numbers of rows and columns of the Hankel matrices, respectively. These values should be chosen large enough to avoid early truncation of the dominant system dynamics, but not so large as to exacerbate noise sensitivity and numerical ill-conditioning. In the noise-free case, $\mathbf{H}_0$ admits the factorization

$$\mathbf{H}_0 = [\mathbf{c}^{\mathrm{T}}, \mathbf{c}^{\mathrm{T}}\mathbf{A}, \ldots, \mathbf{c}^{\mathrm{T}}\mathbf{A}^{r-1}]^{\mathrm{T}}[\mathbf{b}, \mathbf{A}\mathbf{b}, \ldots, \mathbf{A}^{s-1}\mathbf{b}] = \mathcal{O}_r\,\mathcal{C}_s\,,$$

where $\mathcal{O}_r$ and $\mathcal{C}_s$ are the extended observability and controllability matrices, respectively. Consequently, provided that r and s are sufficiently large, the rank of $\mathbf{H}_0$ equals the order of a minimal realization. In practice, however, measurement noise perturbs this exact low-rank structure, so the observed Hankel matrix is generally full rank; the system order must be inferred by separating the dominant modes from the smaller noise-dominated ones.

(a) (b)

Figure 1: Bridge admittance measurement setup. (a) Detail of the dynamometric hammer; (b) violin in place.

The core computational step of ERA is to take the SVD

$$\mathbf{H}_0 = \mathbf{U}\boldsymbol{\Sigma}\mathbf{V}^{\mathrm{T}}. \tag{20}$$

Retaining only the m largest singular values gives the rank-m approximation

$$\mathbf{H}_0 \approx \mathbf{U}_m\boldsymbol{\Sigma}_m\mathbf{V}_m^{\mathrm{T}}\,. \tag{21}$$

where $\boldsymbol{\Sigma}_m = \mathrm{diag}(\sigma_1, \sigma_2, \ldots, \sigma_m)$ contains the m largest singular values of $\mathbf{H}_0$, whereas $\mathbf{U}_m$ and $\mathbf{V}_m$ collect the corresponding left and right singular vectors, respectively. The system parameters are then found as

$$\hat{\mathbf{A}} = \boldsymbol{\Sigma}_m^{-1/2}\mathbf{U}_m^{\mathrm{T}}\mathbf{H}_1\mathbf{V}_m\boldsymbol{\Sigma}_m^{-1/2}\,, \tag{22}$$

$$\hat{\mathbf{b}} = \boldsymbol{\Sigma}_m^{1/2}\mathbf{V}_m^{\mathrm{T}}\mathbf{e}_1^{(s)}\,, \tag{23}$$

$$\hat{\mathbf{c}} = \boldsymbol{\Sigma}_m^{1/2}\mathbf{U}_m^{\mathrm{T}}\mathbf{e}_1^{(r)}\,, \tag{24}$$

$$\hat{d} = y[0]\,, \tag{25}$$

where $\mathbf{e}_1^{(\ell)} = [1, 0, \ldots, 0]^{\mathrm{T}}$ denotes the first canonical basis vector of appropriate dimension ℓ. This formulation, in turn, yields the realization

$$\begin{cases} \hat{\mathbf{x}}[k+1] = \hat{\mathbf{A}}\hat{\mathbf{x}}[k] + \hat{\mathbf{b}}u[k]\,, \\ \hat{y}[k] = \hat{\mathbf{c}}^{\mathrm{T}}\hat{\mathbf{x}}[k] + \hat{d}u[k]\,. \end{cases} \tag{26}$$

This construction uses the shifted Hankel matrix $\mathbf{H}_1 = \mathcal{O}_r\mathbf{A}\mathcal{C}_s$ to recover the state-transition operator and yields a minimum realization when the retained rank matches the true system order; if a smaller rank is retained, it gives a reduced-order approximation. The singular-value truncation is also what makes ERA effective for reduced-order modeling, since it exposes an explicit tradeoff between model complexity and reconstruction fidelity.

In general, ERA yields a dense state matrix. If $\hat{\mathbf{A}}$ is diagonalizable over $\mathbb{C}$, however, (26) can be rewritten in modal form via the eigendecomposition $\hat{\mathbf{A}} = \mathbf{Q}\boldsymbol{\Lambda}\mathbf{Q}^{-1}$ and the change of coordinates

$$\hat{\mathbf{x}} \leftarrow \mathbf{Q}^{-1}\hat{\mathbf{x}}, \quad \hat{\mathbf{A}} \leftarrow \boldsymbol{\Lambda}, \quad \hat{\mathbf{b}} \leftarrow \mathbf{Q}^{-1}\hat{\mathbf{b}}, \quad \hat{\mathbf{c}} \leftarrow \mathbf{Q}^{\mathrm{T}}\hat{\mathbf{c}}\,, \tag{27}$$

yielding a diagonal state matrix as in the state-space design from [3]; see also (3). Unless stated otherwise, the subsequent analysis adopts the modal form of the state-space equations.

4. RESULTS AND DISCUSSION

In this section, we first describe the measurement setup and the acquired data, and then we present the results of our analysis.

4.1. Data Acquisition and Pre-Processing

The study examines a set of six violins, comprising both modern violins made within the 20th and 21st centuries and one historical violin of the 18th century. For all the instruments, the owners provided consent for the usage of the results in an anonymous fashion. For this reason, and for the ease of reading, we will denote the modern violins with f_1–f_5, and we will refer to the historical violin as f_6.

We measure the bridge admittances by means of hammer impact testing. Fig. 1 shows the structure made of wood and rubber bands built to approximate free boundary conditions during the test. Four rubber bands are used for the suspension of the instrument, letting the sample hang in a vertical position and minimizing the contact surface [9, 26]. A dynamometric hammer with a light tip (086E80, by *PCB Piezotronics*) and a uniaxial accelerometer (352A12, by *PCB Piezotronics*) are used to generate an impulsive excitation and measure the harmonic response, respectively. Impacts are applied on one edge of the bridge while the accelerometer is placed on the opposite side. It is worth noting that the hammer tip is fitted with a vinyl impact cap to prevent damage to historical violins; however, this may result in weaker excitation at high frequencies due to the increased contact time.

For each measurement, we acquire six time-domain signals of two seconds sampled at 48 kHz. To obtain the target impulse responses, the accelerometer signals are integrated to obtain velocity signals and normalized by the corresponding force. The responses are then averaged over the number of acquisitions before being processed to obtain minimum-phase sequences with same real cepstrum as the original data. To avoid numerical issues arising from fitting noise, the impulse responses are then cropped to a length L according to their dynamics, within the range $[0.15, 0.30]$ s.

4.2. Implementation of Baseline Methods

We compare the eigensystem realization of the acquired violin bridge admittances against the two methodologies described in Sec. 2. In particular, for [2], i.e., Maestre *et al.* (2013), we set $f_{\text{min}} = 50$ Hz, $f_{\text{max}} = 1300$ Hz, and limit the magnitude spectrum to 6000 Hz. The bridge-hill mode is estimated starting from a smoothed version of the magnitude spectrum obtained considering a Gaussian-weighted moving average filter. As for [3], i.e., Maestre *et al.* (2021), instead, we set $\rho = 0.85$. These parameter choices are consistent with those proposed by the authors and are adopted to ensure a fair and representative comparison.

4.3. Objective Metrics

To assess the performance of ERA against the baseline methods, we run several tests considering three objective metrics. Specifically, we compute the Normalized Mean Squared Error (NMSE) in the time domain, defined as

$$\mathrm{NMSE_t} = \frac{\sum_k (y[k] - \hat{y}[k])^2}{\sum_k y[k]^2} \,. \tag{28}$$

Then, we evaluate the NMSE between magnitude responses

$$\mathrm{NMSE_f} = \frac{\sum_{\omega_k} (|Y[\omega_k]| - |\hat{Y}[\omega_k]|)^2}{\sum_{\omega_k} |Y[\omega_k]|^2} \,. \tag{29}$$

Table 1: Objective metrics for the six violins ($\times 10^{-2}$).

	$\mathrm{NMSE_t}$ (28)			$\mathrm{NMSE_f}$ (29)			$\mathrm{NMAE_{EDR}}$ (30)		
Violin	[2]	[3]	ERA	[2]	[3]	ERA	[2]	[3]	ERA
f_1	38.65	8.13	**1.54**	21.40	4.36	**0.79**	1.14	1.25	**0.79**
f_2	65.78	5.17	**2.13**	44.77	2.59	**1.07**	0.99	1.14	**0.70**
f_3	36.59	9.25	**2.81**	22.05	4.66	**1.47**	1.12	1.11	**0.72**
f_4	31.09	6.11	**2.23**	16.79	3.20	**1.18**	1.18	1.11	**0.62**
f_5	36.97	7.16	**2.09**	20.17	3.84	**1.04**	1.25	1.18	**0.72**
f_6	18.03	6.02	**1.64**	8.39	3.00	**0.85**	1.15	1.16	**0.93**

As a last metric, we consider the Normalized Mean Absolute Error (NMAE) between Energy Decay Relief (EDR) representations, i.e.,

$$\mathrm{NMAE_{EDR}} = \frac{\sum_{t_n} \sum_{\omega_k} |\mathcal{R}[t_n, \omega_k]| - |\hat{\mathcal{R}}[t_n, \omega_k]|}{\sum_{t_n} \sum_{\omega_k} |\mathcal{R}[t_n, \omega_k]|} \,, \tag{30}$$

where the EDR [27] is defined as

$$\mathcal{R}[t_n, \omega_k] = 10 \log_{10} \sum_{t_m = t_n}^{T} |\mathcal{S}[t_m, \omega_k]|^2 \,, \tag{31}$$

with $\mathcal{S}[t_m, \omega_k]$ being the short-time Fourier transform (STFT) of $y[k]$. Here, the STFT in (31) is computed using a 20 ms Hann window, a 1024-point FFT, and a hop length of 5 ms.

4.4. Results

The three metrics are evaluated by varying the model order M in the range $[2, 50]$ with a step of 2, thus considering only the contribution of new resonant modes introduced by complex-conjugate pole pairs. Figs. 2–7 show the results of said analysis, where the blue curve corresponds to Maestre *et al.* (2013), the orange curve to Maestre *et al.* (2021), and the black curve to ERA. The diamonds ($\Diamond$) indicate the model order M that maximizes the aggregated performance across all metrics for both the baseline methods and ERA. Aggregation is performed by summing the three metrics after min–max scaling so as to ensure comparability across scales. The curve corresponding to Maestre *et al.* (2013) is restricted to relatively low values of M, as the peak-picking procedure effectively limits this number of selected modes. Specifically, depending on the admittance under consideration, beyond a certain value of M the number of peaks detected below f_{max} may be insufficient to meet the target order.

Overall, it is always possible to identify a model order M for which ERA achieves the best performance across all considered metrics. For all violins, the errors show a decreasing trend with increasing M, although the behavior is not strictly monotonic, with occasional deviations occurring at specific orders. It is also worth noting that the optimal model order, i.e., the value of M yielding the best overall performance, coincides with $M = 50$ in most cases. Table 1 reports, for each of the six violins, the metrics associated with the orders indicated with diamond markers. Overall, ERA consistently achieves the lowest error values across all metrics and all violins. In particular, a substantial improvement can be observed in terms of $\mathrm{NMSE_t}$, where ERA reduces the error by approximately one order of magnitude with respect to [2], and by a factor of about three to five compared to [3]. A similar trend is observed for $\mathrm{NMSE_f}$ and $\mathrm{NMAE_{EDR}}$, where ERA provides a more accurate reconstruction of the frequency-domain characteristics. This aspect is particularly relevant, as it suggests that ERA

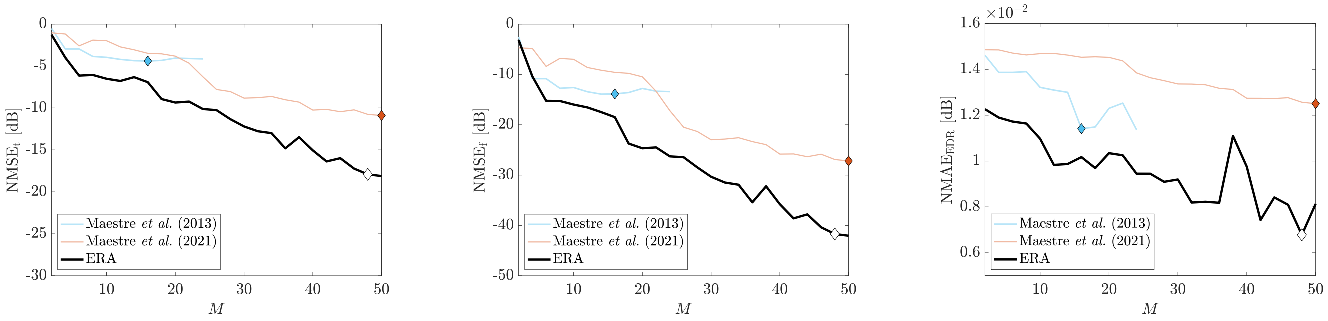

(a) NMSE$_\mathrm{t}$ **(b)** NMSE$_\mathrm{f}$ **(c)** NMAE$_\mathrm{EDR}$

Figure 2: Violin f_1: NMSE$_\mathrm{t}$, NMSE$_\mathrm{f}$, and NMAE$_\mathrm{EDR}$ in dB vs. order M. Diamonds mark the order M for which each method obtains the best performance across all metrics, i.e., $M = 16$ for Maestre *et al.* (2013), $M = 50$ for Maestre *et al.* (2021), and $M = 48$ for ERA.

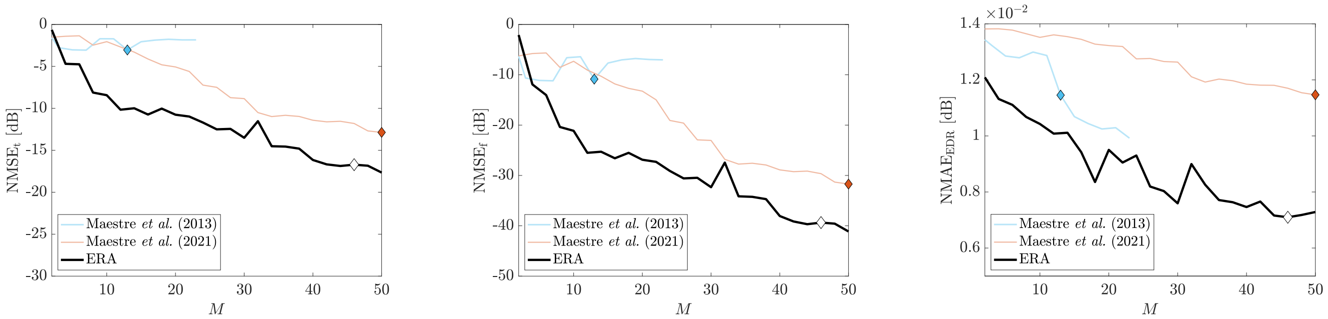

(a) NMSE$_\mathrm{t}$ **(b)** NMSE$_\mathrm{f}$ **(c)** NMAE$_\mathrm{EDR}$

Figure 3: Violin f_2: NMSE$_\mathrm{t}$, NMSE$_\mathrm{f}$, and NMAE$_\mathrm{EDR}$ in dB vs. order M. Diamonds mark the order M for which each method obtains the best performance across all metrics, i.e., $M = 13$ for Maestre *et al.* (2013), $M = 50$ for Maestre *et al.* (2021), and $M = 46$ for ERA.

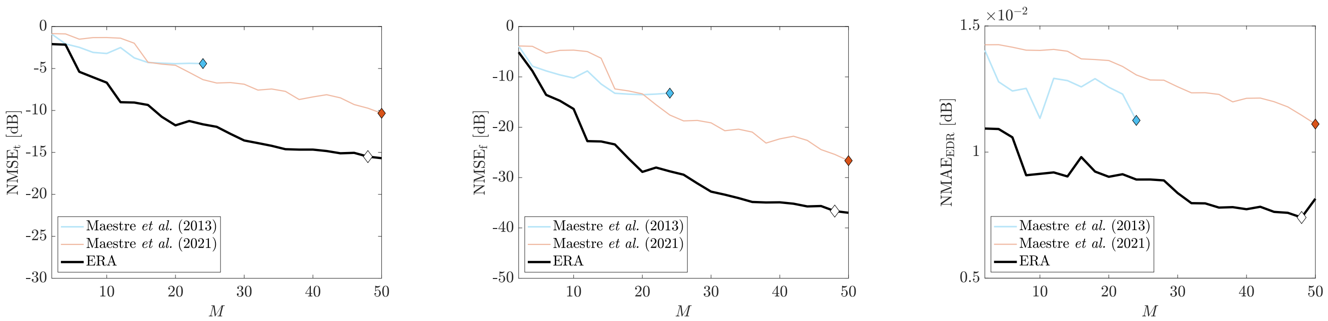

(a) NMSE$_\mathrm{t}$ **(b)** NMSE$_\mathrm{f}$ **(c)** NMAE$_\mathrm{EDR}$

Figure 4: Violin f_3: NMSE$_\mathrm{t}$, NMSE$_\mathrm{f}$, and NMAE$_\mathrm{EDR}$ in dB vs. order M. Diamonds mark the order M for which each method obtains the best performance across all metrics, i.e., $M = 24$ for Maestre *et al.* (2013), $M = 50$ for Maestre *et al.* (2021), and $M = 48$ for ERA.

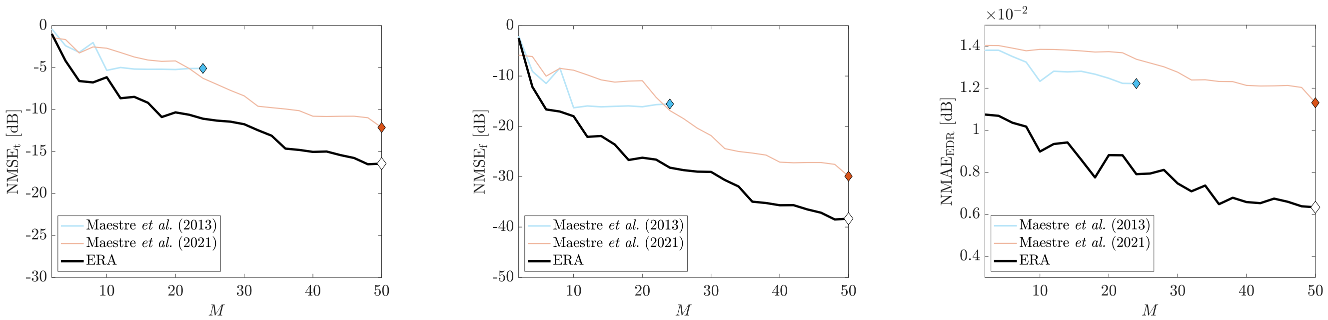

(a) NMSE$_\mathrm{t}$ **(b)** NMSE$_\mathrm{f}$ **(c)** NMAE$_\mathrm{EDR}$

Figure 5: Violin f_4: NMSE$_\mathrm{t}$, NMSE$_\mathrm{f}$, and NMAE$_\mathrm{EDR}$ in dB vs. order M. Diamonds mark the order M for which each method obtains the best performance across all metrics, i.e., $M = 24$ for Maestre *et al.* (2013), $M = 50$ for Maestre *et al.* (2021), and $M = 50$ for ERA.

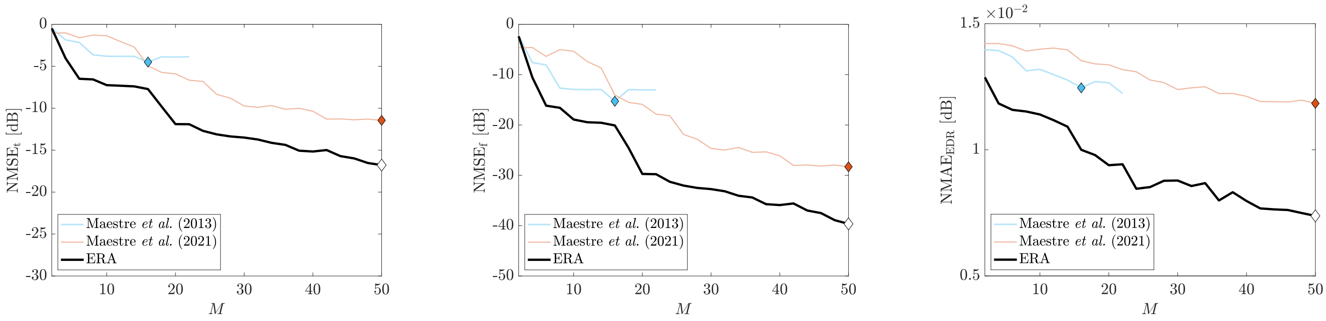

(a) $\mathrm{NMSE_t}$ **(b)** $\mathrm{NMSE_f}$ **(c)** $\mathrm{NMAE_{EDR}}$

Figure 6: Violin f_5: $\mathrm{NMSE_t}$, $\mathrm{NMSE_f}$, and $\mathrm{NMAE_{EDR}}$ in dB vs. order M. Diamonds mark the order M for which each method obtains the best performance across all metrics, i.e., $M = 16$ for Maestre *et al.* (2013), $M = 50$ for Maestre *et al.* (2021), and $M = 50$ for ERA.

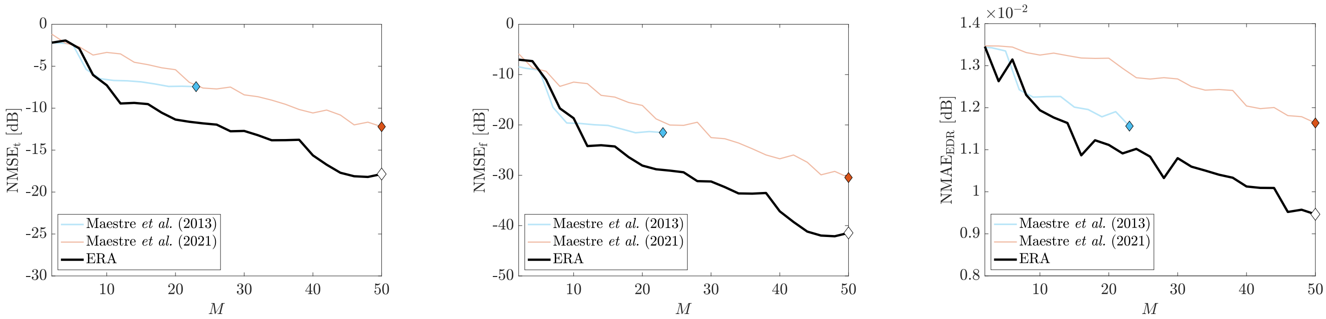

(a) $\mathrm{NMSE_t}$ **(b)** $\mathrm{NMSE_f}$ **(c)** $\mathrm{NMAE_{EDR}}$

Figure 7: Violin f_6: $\mathrm{NMSE_t}$, $\mathrm{NMSE_f}$, and $\mathrm{NMAE_{EDR}}$ in dB vs. order M. Diamonds mark the order M for which each method obtains the best performance across all metrics, i.e., $M = 23$ for Maestre *et al.* (2013), $M = 50$ for Maestre *et al.* (2021), and $M = 50$ for ERA.

not only improves the overall fidelity of the magnitude response but also captures the dynamic behavior of resonances over time.

Fig. 8 shows, as a representative example, the time-domain bridge admittance of violin f_1, comparing the three methodologies against the measured response. To do so, the model order M is set to the value yielding the best performance, namely $M = 16$, $M = 50$, and $M = 48$ for Maestre *et al.* (2013), Maestre *et al.* (2021), and ERA, respectively. While differences in the time domain are not easily distinguishable, apart from the case of Maestre *et al.* (2013) in Fig. 8a, a clearer comparison can be obtained by considering Fig. 9, where the magnitude frequency response of the bridge admittances is reported. While Maestre *et al.* (2021) provides a better match at higher frequencies, particularly above 3 kHz, ERA appears to be the most accurate approach over the range of 200 Hz to 3 kHz, i.e., the frequency band that contains the characteristic resonances of a violin [8]. It is also worth noting that both Maestre *et al.* (2013) and ERA capture a prominent peak at around 130 Hz, likely associated with a structural mode of the mounting system supporting the violin, whereas Maestre *et al.* (2021) does not, possibly due to the effect of frequency warping.

To further evaluate the performance of the three methods, we examine the EDRs reported in Fig. 10. On the one hand, Fig 10a shows that the energy of the target IR persists over time in different frequency bands, with the lower ones reaching -60 dB at around 1 s. On the other hand, none of the modeling methodologies considered in this analysis (Figs. 10b–10d) is capable of fully reproducing the exact decay of energy in the time-frequency domain. Fig. 10b shows almost no energy above 1.5 kHz, while Fig. 10c reveals that, in the same frequency range, the energy rapidly vanishes a few milliseconds after the impulse. Accordingly, both Maestre *et al.* (2013) and Maestre *et al.* (2021) deviate significantly from the target EDR (Fig. 10a). Conversely, Fig. 10d corroborates our previous findings, by showing that ERA is capable of modeling the target violin bridge admittance more accurately than the considered baselines, matching the energy decay more closely at both low and high frequencies.

5. CONCLUSIONS

In this article, we investigated the use of the Eigensystem Realization Algorithm (ERA) for modeling violin bridge admittances from measured impulse responses. The proposed approach was evaluated on a dataset comprising modern and historical instruments and compared against two methodologies of the literature. Results showed that ERA consistently achieved superior performance across all considered metrics, demonstrating improved accuracy in both the time and frequency domains. In particular, ERA was able to better capture the frequency-dependent decay of energy, highlighting its ability to reproduce the dynamic behavior of the instrument beyond standard spectral matching, supporting its use in applications such as sound synthesis, analysis, and instrument virtualization.

6. REFERENCES

[1] U. Zölzer, *DAFX: Digital Audio Effects*, second edition ed. John Wiley and Sons, Mar. 2011.

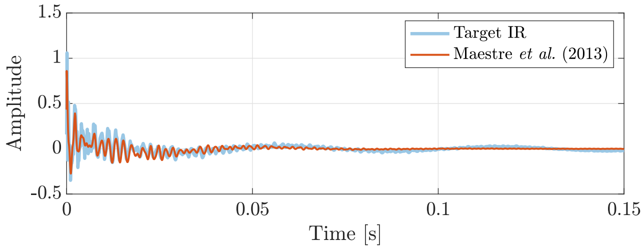

(a)

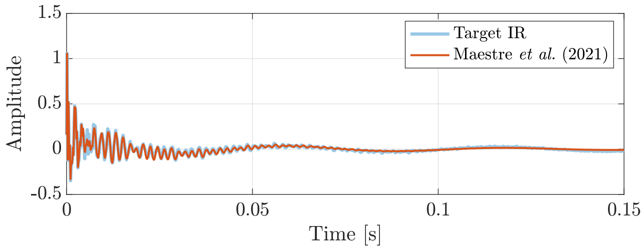

(b)

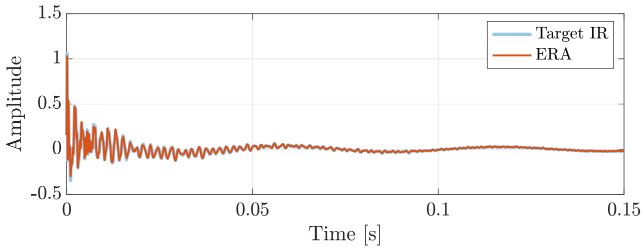

(c)

Figure 8: Violin f_1. Comparison among the impulse response of baseline methods (Maestre et al. (2013), Maestre et al. (2021)) and proposed approach (ERA) and the target violin bridge admittance (Target IR) over the first 150 ms.

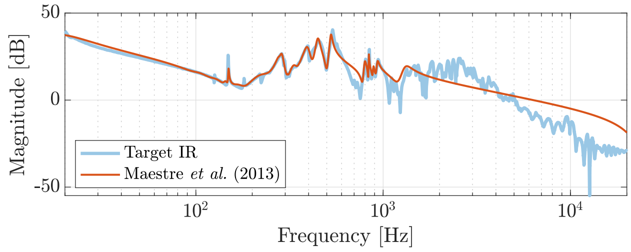

(a)

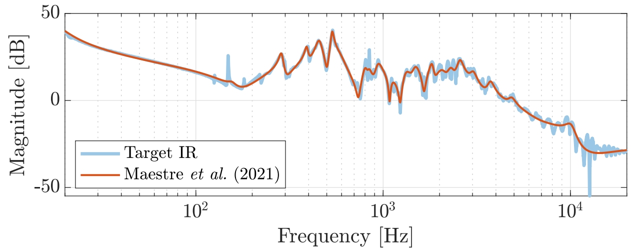

(b)

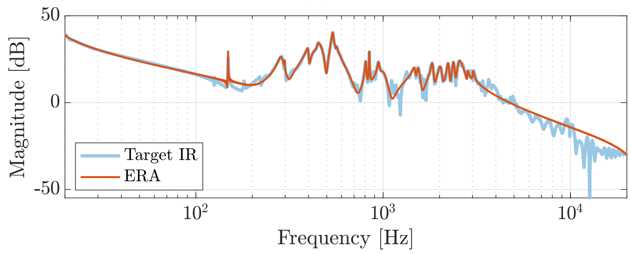

(c)

Figure 9: Violin f_1. Magnitude frequency response of the bridge admittance for the different methods.

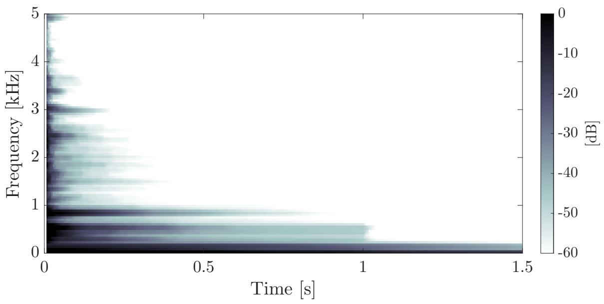

(a) Target IR.

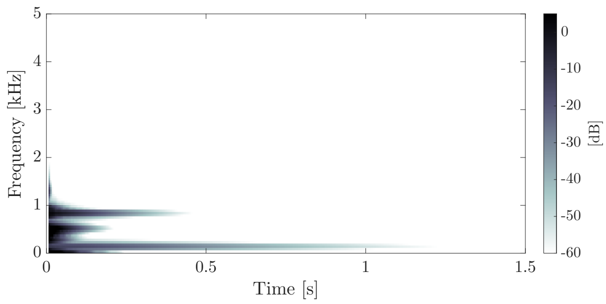

(b) Maestre *et al.* (2013).

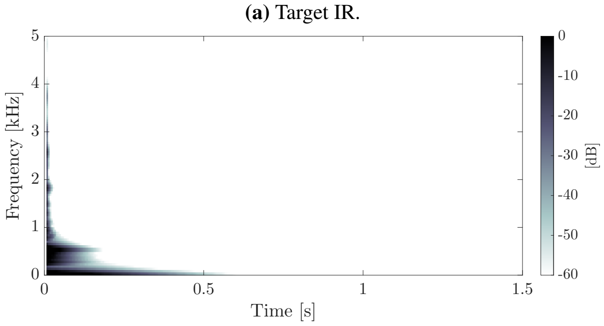

(c) Maestre *et al.* (2021).

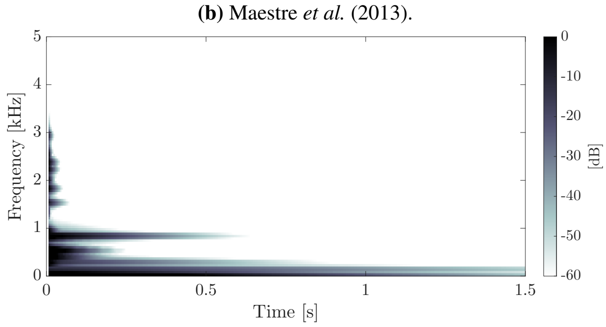

(d) ERA.

Figure 10: Violin f_1. Energy Decay Relief (EDR) of the bridge admittances. Each EDR is normalized to unit Frobenius norm.

[2] E. Maestre, G. P. Scavone, and J. O. Smith III, "Digital Modeling of Bridge Driving-Point Admittances from Measurements on Violin-Family Instruments," in *Proceedings of the Sound and Music Computing Conference (SMC)*, Stockholm, Sweden, Aug. 2013.

[3] E. Maestre, G. P. Scavone, and J. O. Smith, "State-space Modeling of Sound Source Directivity: An Experimental Study of the Violin and the Clarinet," *The Journal of the Acoustical Society of America*, vol. 149, no. 4, pp. 2768–2781, Apr. 2021.

[4] M. Rau, J. S. Abel, J. O. Smith, and D. L. James, "String Instrument Acoustic Transfer Processing," *The Journal of the Acoustical Society of America*, vol. 148, pp. 2643–2643, Oct. 2020.

[5] D. Trueman and P. Cook, "BoSSA: The Deconstructed Violin Reconstructed," *Journal of New Music Research*, vol. 29, no. 2, pp. 121–130, 2000.

[6] J. Woodhouse, "The Acoustics of the Violin: A Review," *Reports on Progress in Physics*, vol. 77, no. 11, p. 115901, 2014.

[7] B. Elie, F. Gautier, and B. David, "Acoustic Signature of Violins Based on Bridge Transfer Mobility Measurements," *The Journal of the Acoustical Society of America*, vol. 136, no. 3, pp. 1385–1393, 2014.

[8] L. Cremer, *The Physics of the Violin*. MIT Press, 1984.

[9] C. Vasques and J. D. Rodrigues, *Vibration and Structural Acoustics Analysis: Current Research and Related Technologies*. Springer Science & Business Media, 2011.

[10] S. Gonzalez, D. Salvi, F. Antonacci, and A. Sarti, "Eigenfrequency Optimisation of Free Violin Plates," *The Journal of the Acoustical Society of America*, vol. 149, no. 3, pp. 1400–1410, Mar. 2021.

[11] M. Rau, J. Smith III, and J. Abel, "A Comparison of Modal Parameter Extraction Methods when Applied to Measurements of Stringed Instruments," in *Proceedings of the 10th Convention of the European Acoustics Association Forum Acusticum 2023*, Turin, Italy, Jan. 2024, pp. 2425–2431.

[12] R. Malvermi, J. S. Gonzalez Briones, M. Quintavalla, F. Antonacci, A. Sarti, J. Torres, R. Corradi *et al.*, "Feature-based Representation for Violin Bridge Admittances," in *Proceedings of the 27th International Congress on Sound and Vibration (ICSV)*, 2021, pp. 1–8.

[13] C. E. Gough, "A Violin Shell Model: Vibrational Modes and Acoustics," *The Journal of the Acoustical Society of America*, vol. 137, no. 3, pp. 1210–1225, 2015.

[14] G. Bissinger, "Structural Acoustics Model of the Violin Radiativity Profile," *The Journal of the Acoustical Society of America*, vol. 124, no. 6, pp. 4013–4023, 2008.

[15] J. Woodhouse and R. Langley, "Interpreting the Input Admittance of Violins and Guitars," *Acta Acustica united with Acustica*, vol. 98, no. 4, pp. 611–628, 2012.

[16] G. Bissinger and J. Keiffer, "Radiation Damping, Efficiency, and Directivity for Violin Normal Modes Below 4 kHz," *Acoustics Research Letters Online*, vol. 4, no. 1, pp. 7–12, 2003.

[17] M. Pezzoli, A. Canclini, F. Antonacci, and A. Sarti, "A Comparative Analysis of the Directional Sound Radiation of Historical Violins," *The Journal of the Acoustical Society of America*, vol. 152, no. 1, pp. 354–367, 2022.

[18] J. O. Smith III, "Efficient Synthesis of Stringed Musical Instruments," in *Proceedings of the International Computer Music Conference*, Toyko, Japan, Sept. 1993, p. 64–71.

[19] B. Bank and M. Karjalainen, "Passive Admittance Matrix Modeling for Guitar Synthesis," in *Proceedings of the 13th International Conference on Digital Audio Effects (DAFx)*, Graz, Austria, 2010.

[20] K. D. Marshall, "Modal Analysis of a Violin," *Journal of the Acoustical Society of America*, vol. 77, pp. 695–709, 1985.

[21] E. Ó Néill, M. Ortiz, and M. van Walstijn, "Tunable Instrument Body Resonances: From Measured Instrument Body Impulse Response to Parametric Convolution," in *Proceedings of the International Computer Music Conference (ICMC)*, Limerick, Ireland, Jul. 2022, pp. 89–92.

[22] M. Karjalainen, "Efficient Realization of Wave Digital Components for Physical Modeling and Sound Synthesis," *IEEE Transactions on Audio, Speech, and Language Processing*, vol. 16, no. 5, pp. 947–956, Jul. 2008.

[23] R. S. Pappa and J.-N. Juang, "Galileo Spacecraft Modal Identification Using an Eigensystem Realization Algorithm," in *Proceedings of the 25th Structures, Structural Dynamics and Materials Conference*, 1984, pp. 630–645.

[24] J.-N. Juang and R. S. Pappa, "An Eigensystem Realization Algorithm for Modal Parameter Identification and Model Reduction," *Journal of Guidance, Control, and Dynamics*, vol. 8, no. 5, pp. 620–627, 1985.

[25] B. L. Ho and R. E. Kálmán, "Effective Construction of Linear State-variable Models from Input/Output Functions," *at-Automatisierungstechnik*, vol. 14, no. 1-12, pp. 545–548, 1966.

[26] T. Kiesel, P. Langer, and S. Marburg, "Numerical Study on the Effect of Gravity on Modal Analysis of Thin-walled Structures," *Acta Acustica united with Acustica*, vol. 105, no. 3, pp. 545–554, 2019.

[27] J.-M. Jot, "An Analysis/Synthesis Approach to Real-Time Artificial Reverberation," in *Proceedings of the 1992 IEEE International Conference on Acoustics, Speech, and Signal Processing (ICASSP)*, vol. 2, 1992, pp. 221–224.